



Special Issue on SMI 2016

Bijective spherical parametrization with low distortion

Chunxue Wang¹, Xin Hu², Xiaoming Fu³, Ligang Liu^{*}

University of Science and Technology of China, 96 Jinzhai Road, Hefei, Anhui 230026, China

ARTICLE INFO

Article history:

Received 10 March 2016

Received in revised form

10 May 2016

Accepted 10 May 2016

Available online 27 May 2016

Keywords:

Bijectivity

Spherical parametrization

Maximal distortion

Inexact block coordinate descent method

ABSTRACT

Computing a bijective spherical parametrization of a genus-0 surface with low distortion is a fundamental task in geometric modeling and processing. Current methods for spherical parametrization cannot, in general, control the worst case distortion of all triangles nor guarantee bijectivity. Given an initial bijective spherical parametrization, with high distortion, we develop a non-linear constrained optimization problem to refine it, with objective penalizing the presence of triangles degeneration and maximal distortion. By using a dynamic adjusting parameter and a constrained, iterative inexact block coordinate descent optimization method, we efficiently and robustly achieve a bijective and low distortion parametrization with an optimal sphere radius. Compared to the state-of-the-art methods, our method is robust to initial parametrization and not sensitive to parameter choice. We demonstrate that our method produces excellent results on numerous models undergoing simple to complex shapes, in comparison to several state-of-the-art methods.

© 2016 Elsevier Ltd. All rights reserved.

1. Introduction

The task of computing a bijective spherical parametrization with low distortion is fundamental in computer graphics, geometric modeling and processing, medical imaging, physical simulations and engineering. For the genus-0 surface, sphere is a natural parametric domain on which we can construct seamless parametric representations directly. A good parametrization $f : M \rightarrow S$ between a genus-0 surface M and a spherical domain S is bijective and with possibly lowest distortion, especially with low maximal distortion. Nevertheless, the problem of producing such a good spherical parametrization is still an open problem.

Computing a spherical parametrization needs image vertices to remain on a sphere whose radius is unknown to user in advance. Bijectivity requires the parametrization to be orientation-preserving. These requirements can be formulated as non-linear constraints and make the problem difficult to solve. Numerous techniques have been developed in the past ten years. For example, the harmonic spherical map is angle-preserving [1–3]. A curvilinear coordinate system was proposed in [4] to reduce area distortion directly. In order to balance angle and area distortions, Wan et al. [5] proposed an efficient spherical parametrization by progressive optimization and Wang et al. [6] develop an as-rigid-

as-possible (ARAP) spherical parametrization method. Unfortunately, these methods are without bijective constraints and may introduce high distortion, even foldovers. On the extreme regions, for example, long and thin protrusion regions (fingers in the hand), worst-case distortion triangles or foldovers usually appear. Recently many locally injective mapping techniques are proposed to keep the orientation of the mesh elements. Bounded distortion mapping methods [7–10] can generate bijective mappings if the boundary has no self-intersections. Sphere is closed and of course without self-intersections. But the non-linear constraints in spherical parametrization make their solver (quadratic programming and/or semidefinite programming) hard to extend. Methods of [11,12] are only for 2D plane domain and not suitable for our propose. MIPS (Most Isometric ParametrizationS)-like methods [13–16] optimize an initial injective/bijective mapping to keep the injectivity/bijectivity and achieve low distortion. AMIPS (Advanced Most Isometric ParametrizationS) method [15] is a powerful method to find a locally injective mapping with low maximal distortion efficiently, but sensitive to initialization and parameter choice. We extend it onto spherical parametrization with an adaptive parameter adjustment scheme.

In this paper, we formulate the AMIPS energy subject to the spherical constraints and develop a rather simple, efficient optimization method to generate a bijective parametrization with low maximal isometric/conformal distortion with an optimal radius. The keys to our method are an adaptive parameter adjustment scheme during the optimization and computing the optimal radius and parametrization results alternately. We denote our method as BLD (Bijective and Low Distortion). Compared to the state-of-the-art

^{*} Corresponding author. Tel.: +86 13956034184.E-mail address: lglu@ustc.edu.cn (L. Liu).¹ Tel.: +86 18705510336.² Tel.: +86 15855129502.³ Tel.: +86 18612037851.

methods [3,5,6,17], we can achieve a bijective spherical parametrization with both lower average and maximal isometric/conformal distortion. The contributions of our work are summarized as follows:

- We introduce a simple method, including a parameter adjustment scheme and an alternately optimization method, to compute bijective parametrization with low distortion efficiently.
- Our method is robust to initial parametrization and not sensitive to parameter choice, which is demonstrated in a series of models undergoing simple to complex geometry.

2. Related work

2.1. Spherical parametrization

Due to its wide applications in graphics and related fields, spherical parametrization is one of the most studied geometry processing problems and a wide set of elegant and powerful algorithms for spherical parametrization is available [18,19]. In the early years, several methods extend the convex combination on planar domain [20,21] to sphere domain [22–24], where some of the linear methods become non-linear regard to distortion. Recently, more and more work focus on low-distortion spherical parametrization. Conformal distortion is probably the most popular distortion measure [1,17,25,2]. In addition, Sheffer et al. [26] proposed a method to measure angle distortion directly where a set of necessary and sufficient conditions are formulated for the spherical angles of the triangulation to form a valid spherical triangulation. However, all methods above cannot guarantee area-preserving, imposing high angle distortion on highly curved surfaces and causing foldovers. Friedel et al. [27] minimize a simple weighted averages of Dirichlet energy and the area energy to get a balance between angle and area preservation. Wan et al. [5] minimize angle and area distortion together with a coarse-to-fine solving scheme and Wang et al. [6] parametrize the genus-0 mesh onto sphere with an optimal radius in an as-rigid-as-possible (ARAP) manner. Nevertheless, the former lacks control over extreme distortions while the latter does not guarantee to avoid inversion. In fact, inverted elements often appear if the parametrization is far from isometry.

2.2. Inversion-free mappings

The authors of [7–10] seek a mapping whose conformal or isometric distortion can be bounded. A maximal convex subspace is constructed and solved by constrained non-linear optimizations. Their method is not suitable for our purpose due to the non-linear constraints of spherical parametrization. Many algorithms formulate the task as a non-linear optimization problem, which requires an inversion-free initialization and the optimization can keep this property. For planar parametrization, the initial map is usually obtained from the Tutte embedding [20,21]. For mesh deformation, the meshes in the rest-pose are usually served as initializations. The MIPS energy [13] and its variants [14–16] or other energies with barrier terms [28,11] are used to prevent simplices degeneration and penalize high distortion. These methods can be extended to spherical parametrization. AMIPS is able to achieve lower maximal distortion, whereas it is sensitive to initial mapping and parameter choice.

2.3. Distortion measurement

Controlling distortion has been a long standing research problem in planar mappings and a variety of distortion measures have been proposed. Sorkine et al. [29] use $\max\{\sigma_1, \sigma_2^{-1}\}$ for computing parametrizations with strictly bounded distortion. The standard 2D MIPS energy [13] measures the conformal distortion of the mapping: $\sigma_1\sigma_2^{-1} + \sigma_2\sigma_1^{-1}$, where σ_1, σ_2 are the singular values of the Jacobian of the mapping associated with a triangle. Other type energies are functionals constructed based on singular value, such as Dirichlet energy $\sigma_1^2 + \sigma_2^2$, Green-Lagrange energy $(\sigma_1 - 1)^2 + (\sigma_2 - 1)^2$ and stretch energy $\max\{\sigma_1, \sigma_2\}$. There are three alternative ways to measure isometric/conformal distortions [30–34]: as similar as possible (ASAP), as rigid as possible (ARAP) and as killing as possible (AKAP). In addition, controlling distortion is widely used in other applications including mesh improvement [35] with $\sigma_1\sigma_3^{-1}$ and volumetric mapping [36] with the combination of $\sigma_1\sigma_3^{-1} + \sigma_3\sigma_1^{-1}\sigma_1\sigma_2\sigma_3 + (\sigma_1\sigma_2\sigma_3)^{-1}$. We develop the modified MIPS energy to spherical parametrization and the resulting mapping has a good control over the maximal isometric distortion.

3. Discrete conformal and isometric mappings

Mappings between surfaces (or manifolds in general) have been well studied in differential and Riemannian geometry [37–39]. However, discrete surfaces are used in geometric processing, so we need the variational calculus on each element to generalize the formulations from continuous to discrete surfaces.

In this paper we consider the mapping $f : \mathbf{M} \rightarrow \mathbf{S}$ where $\mathbf{M} \subset \mathbb{R}^3$ is the input surface mesh and $\mathbf{S} \subset \mathbb{R}^3$ is the spherical mesh. The map f is a piecewise linear mapping. On each triangle $\tau \in \mathbf{M}$, $f_\tau = \mathbf{J}_\tau \mathbf{x} + \mathbf{b}_\tau$ where \mathbf{J}_τ is the Jacobian of f on τ . From the theorem of continuous mapping [40], we can define two energies E_{angle}^τ and E_{area}^τ on $\tau \in \mathbf{M}$ for angle and area preservation:

$$E_{\text{angle}}^\tau = \frac{\|\mathbf{J}_\tau\|_F^2}{|\mathbf{J}_\tau|}, \quad E_{\text{area}}^\tau = |\mathbf{J}_\tau| + \frac{1}{|\mathbf{J}_\tau|}. \quad (1)$$

Where $\|\cdot\|_F$ denotes the Frobenius norm and $|\cdot|$ denotes the determinant. When the singular values of \mathbf{J}_τ are identical, E_{angle}^τ reaches minimum, and f_τ is conformal. When $|\mathbf{J}_\tau| = 1$, E_{area}^τ is optimal and f_τ is equiareal. A mapping is isometric if and only if it is conformal and equiareal. We can define the isometric energy over \mathbf{M} :

$$E^\tau = \alpha E_{\text{angle}}^\tau + (1 - \alpha) E_{\text{area}}^\tau, \quad (2)$$

$$E^{\mathbf{M}} = \sum_{\tau \in \mathbf{M}} E^\tau = \alpha E_{\text{angle}}^{\mathbf{M}} + (1 - \alpha) E_{\text{area}}^{\mathbf{M}}, \quad (3)$$

where $\alpha \in [0, 1]$ is the trade-off between angle and area preservation. In default, we choose $\alpha = 0.5$ for isometric mapping and $\alpha = 1$ for conformal mapping.

Suppose $\mathbf{M} = \{\mathbf{V}, \mathbf{E}, \mathbf{F}\}$, which is an oriented piecewise linear 2-manifold that consists of a set of vertices $\mathbf{V} = \{v_i, i = 0, \dots, N_v - 1\}$, edges $\mathbf{E} = \{e_l, l = 0, \dots, N_e - 1\}$ and oriented triangles (faces) $\mathbf{T} = \{\tau_j, j = 0, \dots, N_\tau - 1\}$. Assume that each 3D original triangle is equipped with three vertices $\mathbf{x}_\tau = \{\mathbf{x}_\tau^0, \mathbf{x}_\tau^1, \mathbf{x}_\tau^2\}$ and the corresponding unknown spherical parametrization coordinates $\mathbf{u}_\tau = \{\mathbf{u}_\tau^0, \mathbf{u}_\tau^1, \mathbf{u}_\tau^2\}$. A_τ and a_τ denote twice of the area of original triangle τ and the parametrized ones respectively. Given this setup, we can derive the formulas for Eq. (1) over \mathbf{M} . Following [40], both terms may be rewritten in terms of the coordinates \mathbf{x} and \mathbf{u} (instead of in terms of the Jacobians) in an explicit form

(in terms of the mesh vertex coordinates):

$$E_{\text{angle}}^{\mathbf{M}}(\mathbf{u}) = \frac{1}{2} \sum_{\tau \in \mathbf{M}} \left(\frac{1}{a_{\tau}} \sum_{i=0}^2 \cot(\theta_{\tau}^i) \|\mathbf{u}_{\tau}^i - \mathbf{u}_{\tau}^{i+1}\|^2 \right), \quad (4)$$

where θ_{τ}^i is the angle opposite to the edge $(\mathbf{x}_{\tau}^i, \mathbf{x}_{\tau}^{i+1})$ in the triangle whose vertices are \mathbf{x}_{τ} and superscripts are all modulo 3.

$$E_{\text{area}}^{\mathbf{M}}(\mathbf{u}) = \frac{1}{2} \sum_{\tau \in \mathbf{M}} \left(\frac{A_{\tau}}{a_{\tau}(\mathbf{u}_{\tau})} + \frac{a_{\tau}(\mathbf{u}_{\tau})}{A_{\tau}} \right), \quad (5)$$

where $a_{\tau}(\cdot)$ denotes the area of the parametrized triangle \mathbf{u}_{τ} .

Remark 1. E_{angle}^{τ} is 1/2 times inverse mean-ratio metric [41–43]. The energy E_{angle} has been studied in many applications of surfaces and manifolds: harmonic mapping in [44], mesh quality optimization in [45], and the MIPS energy for conformal parametrization in [13] and Dirichlet integral [46] of per parameter area. It is clear that if a degenerated triangle τ appears, $E_{\text{angle}}^{\tau} = E_{\text{area}}^{\tau} = \infty$. From Eq. (1), E_{angle}^{τ} and E_{area}^{τ} both achieve their lowest value 2.

4. Bijective spherical parametrization

In this section, we first formulate the optimization for bijective spherical parametrization in Section 4.1, then present a simple two-step iterative algorithm to solve it in Section 4.2.

4.1. Formulation definition

The radius of parametrization sphere r affects the area distortion. To make the isometric distortion as low as possible, the radius of sphere r is considered during the optimization. Thus, we would like to define the following constrained non-linear optimization problem for parametrization:

$$\begin{aligned} \min_{\mathbf{u}, r} \quad & E^{\mathbf{M}}(\mathbf{u}, r), \\ \text{s.t.} \quad & \|\mathbf{u}_i\|^2 = r^2, \quad i = 0, \dots, N_v - 1. \end{aligned} \quad (6)$$

where $E^{\mathbf{M}}$ is shown in Eq. (3) and $r = 1.0$ for conformal parametrization. Optimizing this problem can achieve small average distortion efficiently. However, it produces some high distortion mesh elements. In other words, it is not capable of controlling the maximal distortion despite a low average distortion. As we all know, producing spherical parametrization of genus-0 surface with low maximal distortion is important in geometric processing/modelling, physical simulations and numerical analysis. Bounded distortions have been studied in [47,7,8] for planar/volume parametrizations/deformations. They are hard to be extended to spherical parametrizations. To the best of our knowledge, algorithms with low maximal distortion for spherical parametrizations have not been developed. To suppress the worst-case distortion, we combine an exponential function with E^{τ} (called AMIPS in [15]). The energy functions are defined as follows:

$$\begin{aligned} \min_{\mathbf{u}, r} \quad & E^s(\mathbf{u}, r) = \sum_{\tau \in \mathbf{M}} \exp(s \cdot E^{\tau}), \\ \text{s.t.} \quad & \|\mathbf{u}_i\|^2 = r^2, \quad i = 0, \dots, N_v - 1. \end{aligned} \quad (7)$$

where s is a parameter controlling the penalty for distortion. Generally, a small s has little effect on penalizing the maximal distortion, and a large s causes numerical instability. Fig. 1 shows the influence on the maximal isometric distortion and average isometric distortion on Hand model. This figure shows that, given a distorted input, the maximal isometric distortion decreases rapidly as s increases, while average isometric distortion decreases at the beginning, then it will increase slightly. This is because as s varies, average isometric distortion is sacrificed to get lower

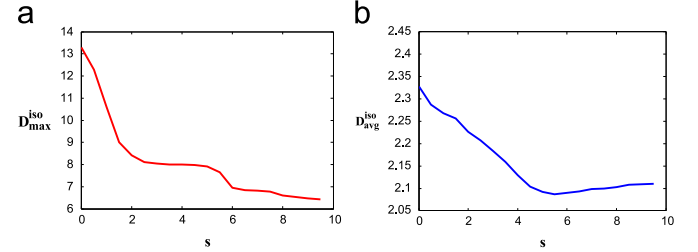


Fig. 1. (a) Maximal isometric distortion D_{\max}^{iso} with respect to s with the range (0,10) on the Hand model. (b) Average isometric distortion $D_{\text{avg}}^{\text{iso}}$ with respect to s with the range (0,10) on the Hand model. D^{iso} is defined in Eq. (12) and the Hand model in Fig. 9.

maximal isometric distortion. Based on this observation, in our implementation, s is adaptively increasing during the optimization, which is described in Section 4.2 in detail.

4.2. Numerical optimization

The algorithm starts with a valid bijective spherical parametrization, for instance, we use the harmonic spherical parametrization [24] on the unit sphere. In most cases there are high distortion triangles for isometric parametrization on the initial sphere. We proposed the following scheme and efficiently to reduce the maximal distortion significantly without inducing numerical instability.

1. We use the optimization Eq. (6) in the first 100 iterations. It helps us to decrease the distortion efficiently on each element instead of those on the extreme elements since the each element of initial guess is far from isometry/conformal. It is necessary enough to decrease both the average and maximal distortion significantly.
2. s is adaptively increased during the optimization. While a bijective initial guess with extremely high distortion is given, a default $s=5$ used in [15] may make the solver trapped in local minimum, and output an unsatisfactory result. In our implementation, we change s from 0.1 to 10.

It is non-trivial to solve such a non-linear problem with non-linear constraints mentioned in Eqs. (6) and (7). Observing that the non-linear optimization problems Eqs. (6) and (7) couple the optimal radius r and spherical parametrization coordinates \mathbf{u} together, we develop a two-step iterative algorithm updating the variables separately.

Starting from a valid initial spherical parametrization from any available algorithm, which may produce extremely large distortion, our algorithm alternatively updates r and \mathbf{u} to return a bijective spherical parametrization with low distortion. The two-step iterative algorithm is described as follows.

4.2.1. Optimizing \mathbf{u}

Based on the locality of energy in Eqs. (6) and (7) and given a radius r , we efficiently update \mathbf{u} with inexact BCD (block coordinate descent) method [48,15] (details can be found in Appendix A). The algorithm is as follows.

A bijective initial spherical parametrization from any available algorithm should work well. Our method is insensitive to different initializations (See Section 5.1). In default, we set the harmonic spherical parametrization [24] on unit sphere as the initial bijective parametrization.

Given the sphere of radius r , we update each vertex \mathbf{u}_v by one step of gradient descent:

$$\mathbf{u}_v^{(k+1)} = \mathbf{u}_v^{(k)} - \alpha_v \nabla_{\mathbf{u}_v} E^{\star}, \quad (8)$$

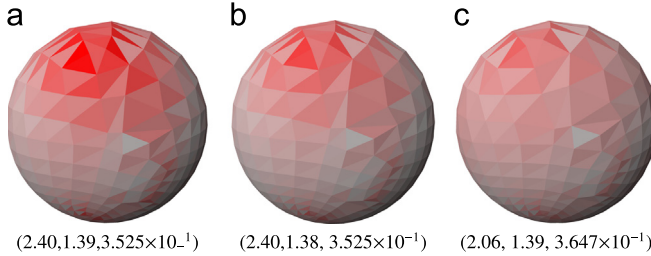


Fig. 2. Comparison of different schemes on radius update. (a) shows a result of radius r_0 in Eq. (10); (b) shows a result of radius update with the second scheme in Eq. (9) from an initial radius r_0 of Eq. (10); (c) shows a result of radius update with the first scheme in Eq. (11) from an initial radius r_0 of Eq. (10). The numbers below the figure are D_{max}^{iso} , D_{avg}^{iso} and radius respectively.

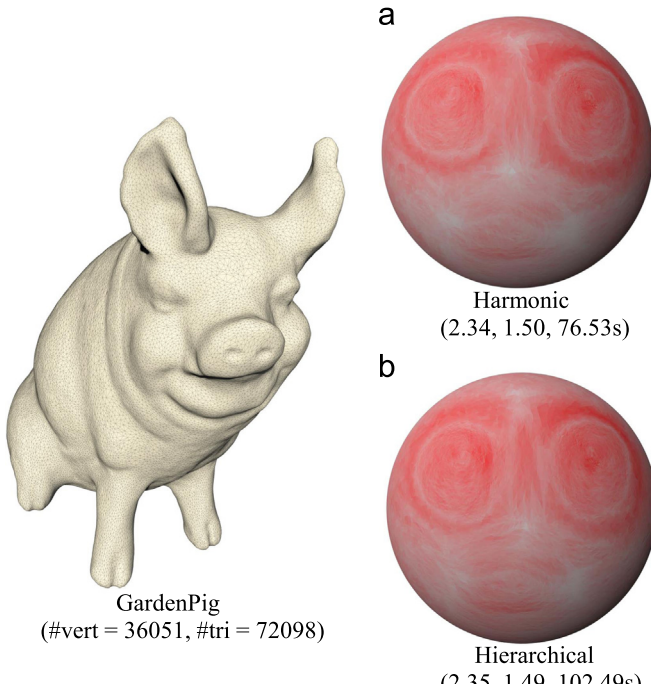


Fig. 3. Comparison of our parametrization results with different initial guesses. (a) Initialized with the Harmonic parametrization [24]; (b) initialized with the Hierarchical parametrization [5]. The color encodes the isometric distortion D^{iso} defined in Eq. (12). Numbers in bracket denote D_{max}^{iso} , D_{avg}^{iso} and running time (in seconds) respectively.

where α_v is the step length we need to determine and E^* represents $E^M(\mathbf{u}, r)$ in Eq. (6) and $E^S(\mathbf{u}, r)$ in Eq. (7). $\nabla_{\mathbf{u}_v} E^*$ is computed in Appendix B in detail. The initial α_v is obtained by normalizing the $\nabla_{\mathbf{u}_v} E^*$ to the minimal neighboring edge length of \mathbf{u}_v . $\mathbf{u}_v^{(k+1)}$ is projected onto the sphere of radius r_k . The one step of gradient descent stops when the energy decreases and there is not any inverted vertex in the neighbors of vertex \mathbf{u}_v . If not, we reduce α_v by 0.8 and normalize $\mathbf{u}_v^{(k+1)}$ to the length of r_k until both conditions are satisfied. When α_v is less than 10^{-10} , we set $\mathbf{u}_v^{(k+1)} = \mathbf{u}_v^{(k)}$ and $k = k + 1$. The key to success is to ensure the vertex on the sphere of r_k and to decrease the energy without self-intersections.

Our algorithm terminates when the relative error of the energy value is less than 10^{-5} and that of the radius value is less than 10^{-3} , or the iteration number exceeds the maximal iteration number.

Remark 2. Different from ARAP [6], where spherical constraints are satisfied by projecting the updated vertex to the sphere of

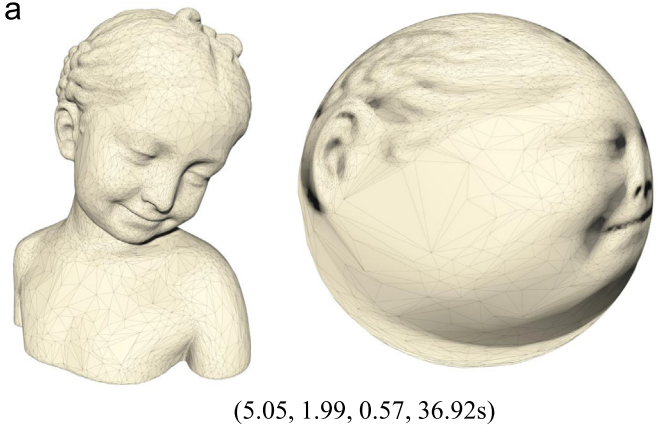


Fig. 4. Models with different tessellations produce approximate metric distortions. (a) The original Bimba model and its BLD result; (b) the re-meshed Bimba model and its BLD result. Numbers in bracket below the figure denote D_{max}^{iso} , D_{avg}^{iso} , D_{dev}^{iso} and running time (in seconds) respectively.

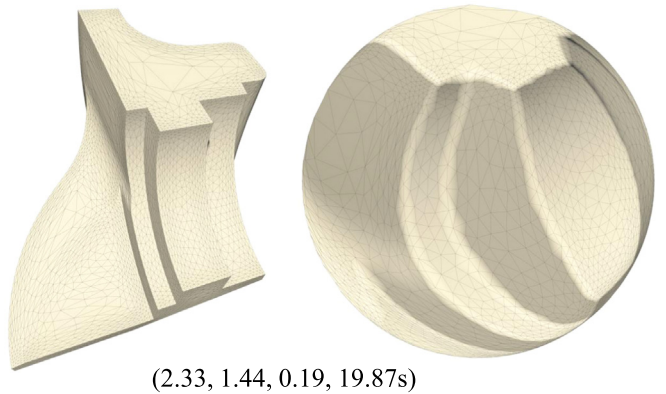


Fig. 5. The model with a tessellation that varies in element size. Numbers in bracket below the figure denote D_{max}^{iso} , D_{avg}^{iso} , D_{dev}^{iso} and running time (in seconds) respectively.

radius r_k after energy optimization, our search strategy is used by checking $\mathbf{u}_v^{(k+1)}$ on the sphere of radius r_k whether decreases the energy and introduces self-intersections in its neighbors.

4.2.2. Optimizing sphere radius r

Commonly, decreasing the area distortion is a necessary condition to decrease isometric distortion, a small or big value of r usually yields large area distortion, thus large isometric distortion. Therefore, finding a sphere with an optimal radius is important for

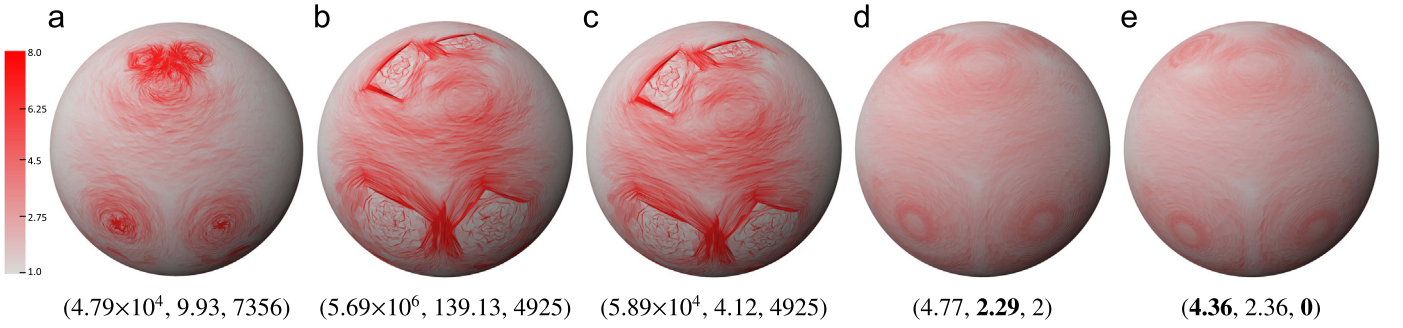


Fig. 6. Performance of our parameter adjustment scheme on the Cow model in Fig. 9. (a) Optimization (6) in the first 100 iterations; (b) optimization (7) with $s = 5$ for 2000 iterations; (c) optimization (7) with $s = 0.1$ for 2000 iterations; (d) optimization (7) with s -adjustment from 0.1 to 10 for 2000 iterations; (e) optimization (6) in the first 100 iterations, then optimization (7) with s -adjustment from 0.1 to 10 for 1900 iterations. The color encodes the isometric distortion D^{iso} defined in Eq. (12). The numbers in brackets below the figure are D_{max}^{iso} , D_{avg}^{iso} and the number of triangles whose isometric distortion is greater than the maximal isometric distortion of (e).

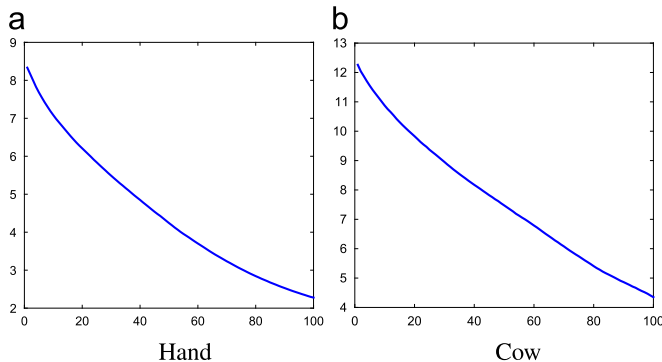


Fig. 7. Log-scale of energy (per triangle) with respect to iterations on Hand model and Cow model in Fig. 9. The y-axis shows the log-scale of energy and The x-axis shows the iteration number.

isometric spherical parametrization. The radius r has a direct influence on the distribution of distortion, so updating r should guide the penalty of isometric distortion efficiently.

There are two direct methods to optimize radius.

1. The radius is treated as a variable to be optimized directly.
2. Another way for updating radius is to keep the area of the original surface through the parametrization.

But the initial mapping with too large distortion may cause the first scheme to be trapped easily. In our method, we first use the second scheme to optimize radius until the algorithm converges, then the first scheme is applied to further reduce area distortion.

The radius updating formulation of the second scheme is defined as follows.

$$r^{(k+1)} = \sqrt{\frac{\sum_{\tau} A_{\tau}}{\sum_{\tau} a_{\tau}^{(k)}}} r^{(k)}, \quad (9)$$

where $r^{(k)}$ is the value of r after its k th update, and $a_{\tau}^{(k)}$ is the area of triangle τ after its k th update in spherical parametrization. To avoid large area distortion in the first few steps, we set the initial radius r as

$$r^{(0)} = \sqrt{\frac{\sum_{\tau} A_{\tau}}{4\pi}}, \quad (10)$$

The updating method of the first scheme is to optimize area distortion Eq. (6) directly. $r^{(k+1)}$ can be obtained directly:

$$r^{(k+1)} = \left(\sum_{\tau \in M} \frac{A_{\tau}}{a_{\tau}^{(k)}} \right) \left/ \sum_{\tau \in M} \frac{a_{\tau}^{(k)}}{A_{\tau}} \right. \right)^{\frac{1}{4}} \cdot r^{(k)}, \quad (11)$$

Fig. 2 shows a comparison of different schemes and shows that the first scheme always achieves both lower maximal distortion and average distortion.

4.3. Bijectivity

Our goal is to produce a bijective spherical parametrization from a 3D genus-0 mesh to a sphere. A parametrization for a triangular mesh is bijective if two conditions hold [49,16]:

- (a) The parametrization is inversion-free.
- (b) The parametrization of boundary is a bijective map, i.e. the boundary of parametrization does not intersect itself.

An inversion-free map is guaranteed by minimizing the energy E^M . Since our original mesh is a closed one, that is, the original mesh has no boundary. Condition (a) is sufficient to guarantee a bijective spherical parametrization, based on the two-step iterative algorithm in Section 4.2.

5. Experimental results and comparison

We test our method (BLD) on series of models undergoing simple to complex shapes, and compare it with the state-of-the-art algorithms including harmonic parametrization (Harmonic) [24], conformal parametrization (Conformal) [17], hierarchical parametrization (Hierarchical) [5] and as-rigid-as-possible spherical parametrization (ARAP) [6]. For both Conformal and Hierarchical methods, we use the authors' implementation in our experiments. All models in our paper are normalized the bounding box to unit length for comparisons and we use the Harmonic results as initializations for all models.

Notice that the energy in Eqs. (6) and (7) defined on a vertex only involves its neighboring vertices, we group the disconnected vertices into a block which can be updated simultaneously. To realize this, we use the standard graph coloring algorithm in Boost

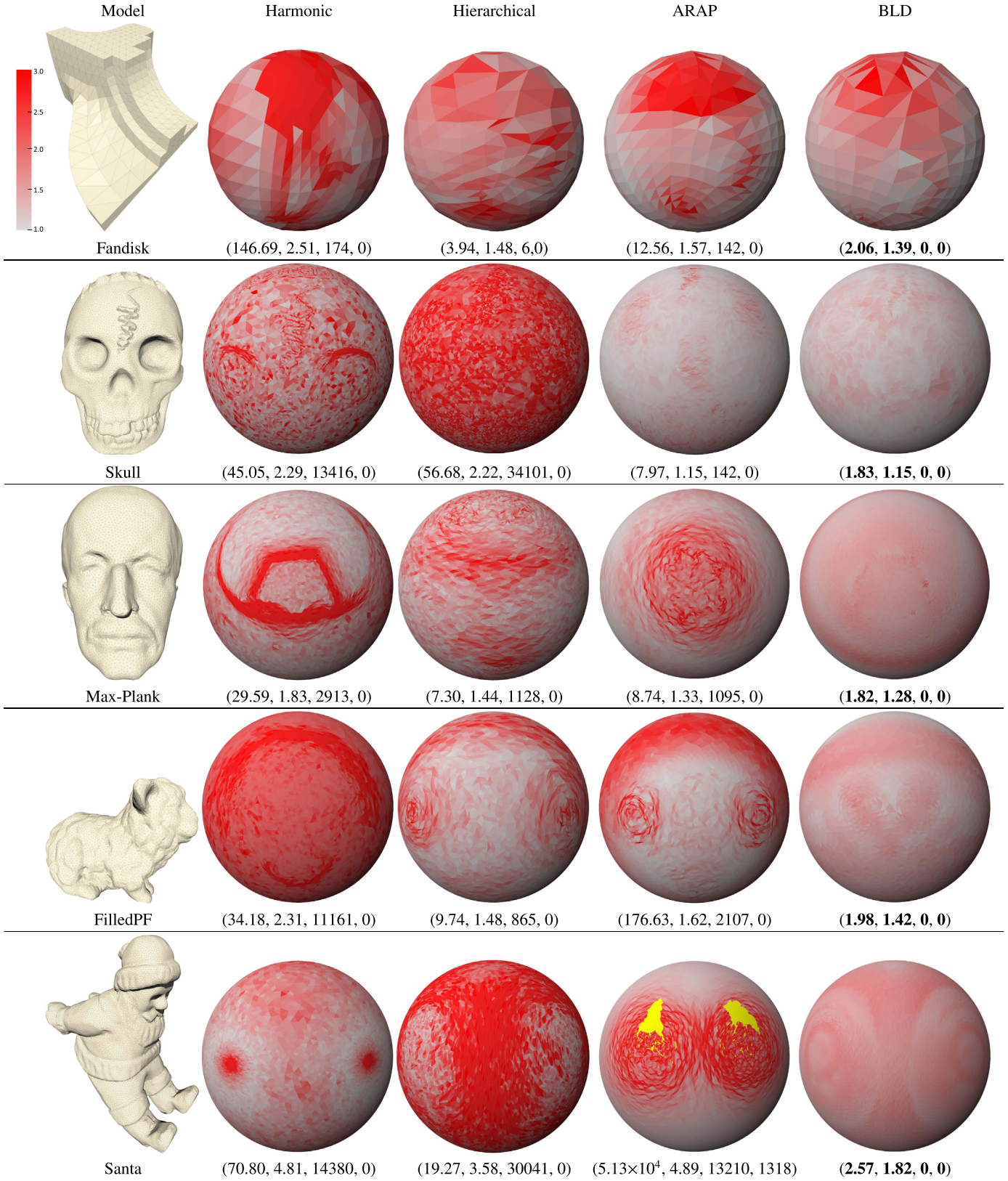


Fig. 8. Spherical parametrizations of five simple models using Harmonic, Hierarchical, ARAP and BLD. The color encodes the isometric distortion D^{iso} and yellow faces highlight inverted. The numbers in bracket below the figure are D_{max}^{iso} , D_{avg}^{iso} , number of triangles whose isometric distortion is greater than the maximal isometric distortion of BLD and number of inverted triangles respectively.

Graph library. To implement our algorithm efficiently, we parallelize our inexact BCD method using OpenMP in C++ on a desktop PC with a 3.3 GHz Intel Core i3 and 8 GB RAM, which is

about 2–3 times faster than the serialized version. We ensure that better performance can be obtained on a higher configured computer.

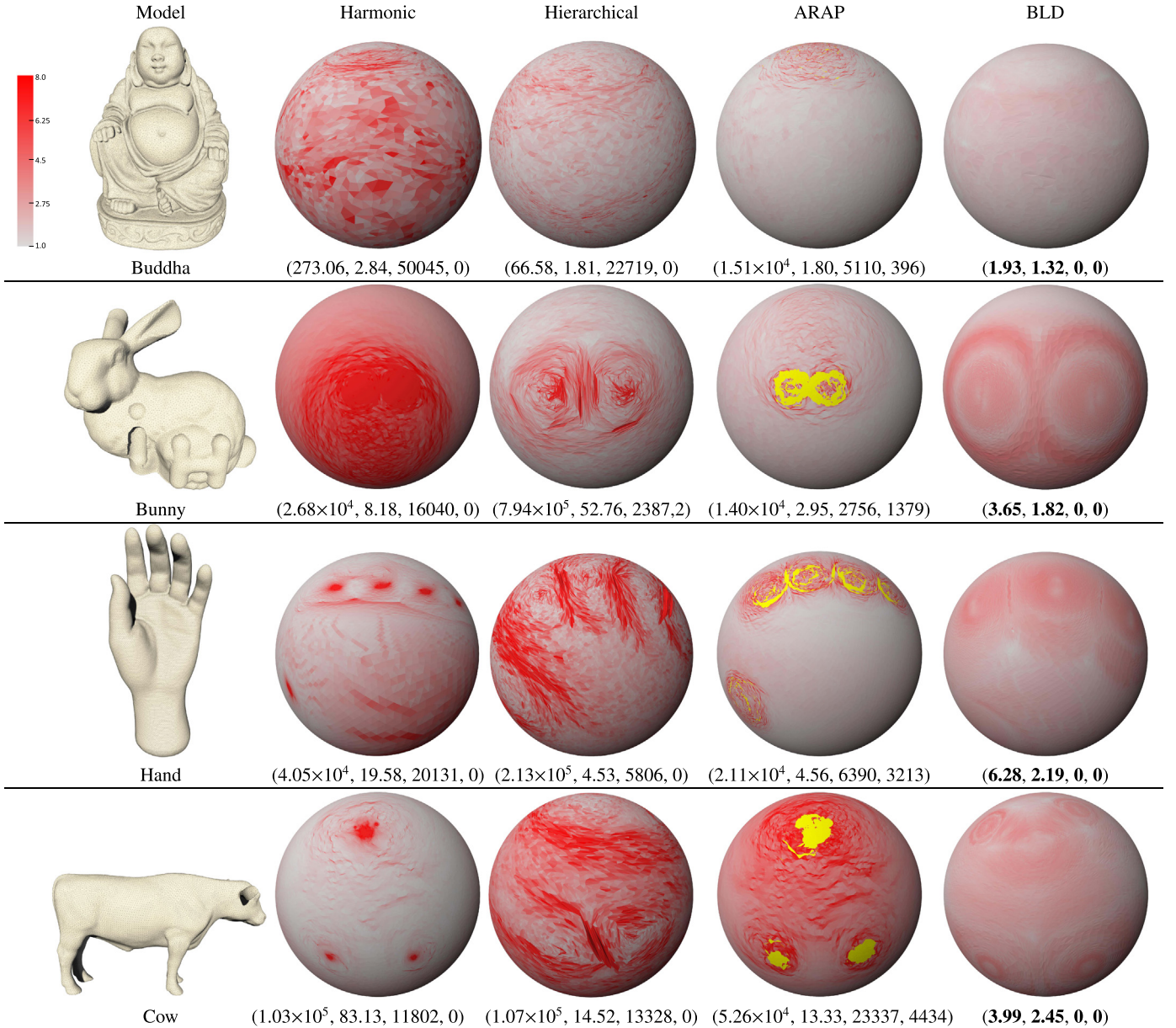


Fig. 9. Spherical parametrizations of four complex models using Harmonic, Hierarchical, ARAP and BLD. The color encodes the isometric distortion D_{τ}^{iso} and yellow faces highlight inverted. The numbers below the figure are D_{\max}^{iso} , $D_{\text{avg}}^{\text{iso}}$, number of triangles whose isometric distortion is greater than the maximal isometric distortion of BLD and number of inverted triangles respectively.

Distortion metrics: Different distortion metrics are defined to quantify the spherical parametrization. Denote $\sigma_{1,\tau}, \sigma_{2,\tau}$ as the signed singular values of Jacobians $J_\tau (\sigma_{1,\tau} < \sigma_{2,\tau})$, following Sorkine et al. [29], we define the isometric distortion of triangle τ as follows:

$$D_{\tau}^{\text{iso}} = \max\{\sigma_{2,\tau}, \sigma_{1,\tau}^{-1}\}, \quad (12)$$

which can penalize the shrinking distortion (i.e. $\sigma_{1,\tau} \rightarrow 0$) better than $(\sigma_{1,\tau} - 1)^2 + (\sigma_{2,\tau} - 1)^2$ in [6]. D_{τ}^{iso} reaches the minimum 1 when both singular values are 1.

Similarly, we define the area distortion and angle distortion as follows:

$$D_{\tau}^{\text{area}} = \sigma_{1,\tau} \sigma_{2,\tau} + 1 / \sigma_{1,\tau} \sigma_{2,\tau}, \quad (13)$$

$$D_{\tau}^{\text{angle}} = \sigma_{1,\tau} / \sigma_{2,\tau} + \sigma_{2,\tau} / \sigma_{1,\tau}. \quad (14)$$

Obviously, the minimum of D_{τ}^{area} and D_{τ}^{angle} are both 2.

We report their maximum, average and standard deviation over the whole surface, denoted as $D_{\max}^{\text{iso}}, D_{\text{avg}}^{\text{iso}}, D_{\text{dev}}^{\text{iso}}, D_{\max}^{\text{area}}, D_{\text{avg}}^{\text{area}}, D_{\text{dev}}^{\text{area}}, D_{\max}^{\text{angle}}, D_{\text{avg}}^{\text{angle}}, D_{\text{dev}}^{\text{angle}}$. To visualize the D_{τ}^{iso} and D_{τ}^{angle} over the mesh, we use the color-coding patterns in Figs. 8-upperleft, 9-upperleft and 11-upperleft and set the best values in bold.

5.1. Robustness to various initializations

An initial bijective spherical parametrization result from any available algorithm is required to input. To test the sensitivity of our method to initializations, we use Harmonic [24] and Hierarchical [5] as two initializations, and make a comparison on the two results in Fig. 3. From the results we can see that almost the same parametrization results produced by our algorithm with different initializations.

Table 1

Statistics and timings on isometric spherical parametrization. Models are from Figs. 8 and 9 respectively, #vert and #tri denote the number of vertices and triangles of the original mesh respectively, each distortion metrics are defined in Eqs. (12) and (13), #FO denotes the number of inverted faces, and the last column shows the timings of each method.

Model	#vert/#tri	$D_{max}^{iso}/D_{avg}^{iso}/D_{dev}^{iso}$	$D_{max}^{area}/D_{avg}^{area}/D_{dev}^{area}$	$D_{max}^{angle}/D_{avg}^{angle}/D_{dev}^{angle}$	#FO	Time(s)
Fandisk-Harmonic	606/1208	146.69/2.51 /4.42	357.55/4.49/10.94	60.04/2.56/1.83	0	5.87
Fandisk-Hierarchical	606/1208	3.94/1.48/0.27	2.81/2.03/0.10	6.64/2.52/0.49	0	–
Fandisk-ARAP	606/1208	12.56/1.57/0.57	15.43/2.41/0.68	10.36/ 2.20 /0.36	0	10.79
Fandisk-BLD	606/1208	2.06/1.39/0.20	3.01/2.07/0.14	2.98/2.24/0.18	0	0.63
Skull-Harmonic	20 002/40 000	45.05/2.29 /1.02	144.61/3.52/2.63	69.38/2.43/0.74	0	63.88
Skull-Hierarchical	20 002/40 000	56.68/2.22/0.88	44.78/3.44/0.89	256.29/2.35/2.37	0	–
Skull-ARAP	20 002/40 000	7.97/ 1.15 /0.16	8.57/2.04/0.11	11.55/ 2.02 /0.10	0	703.09
Skull-BLD	20 002/40 000	1.83/1.15/0.08	2.30/2.02/0.02	2.69/2.04/0.04	0	32.44
Max-Plank-Harmonic	15 000/29 996	29.59/1.83 /0.65	19.68/2.90/1.15	56.51/2.27/0.75	0	125.76
Max-Plank-Hierarchical	15 000/29 996	7.30/1.44/0.29	8.08/2.07/0.16	11.62/2.40/0.51	0	–
Max-Plank-ARAP	15 000/29 996	8.74/1.33/0.31	10.07/2.18/0.36	7.79/ 2.08 /0.15	0	655.93
Max-Plank-BLD	15 000/29 996	1.82/1.28/0.15	2.62/2.06/0.09	2.55/2.11/0.13	0	29.20
FilledPF-Harmonic	7994/15 984	34.18/2.31 /1.18	137.02/4.28/4.39	23.75/2.35/0.69	0	55.76
FilledPF-Hierarchical	7994/15 984	9.74/1.48/0.33	12.06/ 2.05 /0.20	8.04/2.51/0.58	0	–
FilledPF-ARAP	7994/15 984	176.63/1.62/1.99	145.42/2.53/1.73	222.68/ 2.18 /2.33	0	114.61
FilledPF-BLD	7994/15 984	1.98/1.42/0.19	2.91/2.12/0.11	2.87/2.19/0.16	0	15.80
Santa-Harmonic	20 000/39 996	70.80/4.81 /6.80	$3.05 \times 10^4/48.80/191.50$	7.63/ 2.21 /0.23	0	89.05
Santa-Hierarchical	20 000/39 996	19.27/3.58/1.20	11.18/4.85/1.36	67.18/3.53/1.92	0	–
Santa-ARAP	20 000/39 996	$5.13 \times 10^4/4.89/35.46$	$8.71 \times 10^4/8.00/60.13$	$3.02 \times 10^4/3.95/21.53$	1.32×10^4	726.10
Santa-BLD	20 000/39 996	2.57/1.82/0.26	3.75/2.31/0.34	4.03/2.63/0.12	0	42.45
Buddha-Harmonic	44 973/89 942	273.06/2.84 /2.76	743.33/3.79/4.78	211.21/3.39/3.15	0	146.04
Buddha-Hierarchical	44 973/89 942	66.58/1.81/0.83	32.22/2.16/0.35	$1.34 \times 10^4/3.01/5.31$	0	–
Buddha-ARAP	44 973/89 942	$1.51 \times 10^4/1.80/9.25$	$1.76 \times 10^4/2.62/10.08$	$1.29 \times 10^4/2.45/8.89$	396.45	1.03×10^4
Buddha-BLD	44 973/89 942	1.93/1.32/0.14	2.81/2.09/0.09	2.83/2.12/0.10	0	76.95
Bunny-Harmonic	20 002/40 000	$2.68 \times 10^4/8.18/37.47$	$9.32 \times 10^5/237.07/692.01$	208.61/ 2.31 /1.63	0	160.27
Bunny-Hierarchical	20 002/40 000	$7.94 \times 10^5/52.76/1.01 \times 10^4$	$8.52 \times 10^6/1.66 \times 10^4/7.45 \times 10^5$	$2.20 \times 10^5/8.88/166.41$	0	–
Bunny-ARAP	20 002/40 000	$1.40 \times 10^4/2.95/18.49$	$2.31 \times 10^4/3.93/22.20$	$1.28 \times 10^4/3.50/16.54$	1.38×10^4	708.89
Bunny-BLD	20 002/40 000	3.65/1.82/0.55	5.22/2.36/0.59	5.41/2.59/0.70	0	80.47
Hand-Harmonic	42 068/84 132	$4.05 \times 10^4/19.58/14.51$	$4.36 \times 10^6/2.30 \times 10^4/1.61 \times 10^5$	$7.79 \times 10^4/2.56/26.99$	0	662.73
Hand-Hierarchical	42 068/84 132	$2.13 \times 10^5/4.53/90.13$	$3.09 \times 10^5/9.66/1.44 \times 10^4$	$1.08 \times 10^5/5.96/67.07$	0	–
Hand-ARAP	42 068/84 132	$2.11 \times 10^4/4.56/19.83$	$2.60 \times 10^4/5.32/21.08$	$1.72 \times 10^4/5.01/19.44$	3.21×10^4	1.25×10^4
Hand-BLD	42 068/84 132	6.28/2.19/0.34	6.49/2.52/0.47	6.57/3.07/0.69	0	194.47
Cow-Harmonic	23 023/46 042	$1.03 \times 10^5/83.13/468.86$	$3.93 \times 10^7/9.67 \times 10^5/8.77 \times 10^6$	307.75/ 2.29 /2.07	0	634.52
Cow-Hierarchical	23 023/46 042	$1.07 \times 10^5/14.52/168.11$	$1.38 \times 10^6/80.03/1.36 \times 10^4$	$1.04 \times 10^6/7.87/91.54$	0	–
Cow-ARAP	23 023/46 042	$5.26 \times 10^4/13.33/76.79$	$1.61 \times 10^5/38.53/226.63$	$1.76 \times 10^4/5.40/26.81$	4.43×10^4	1.68×10^4
Cow +-BLD	23 023/46 042	3.99/2.45/0.48	6.28/2.49/0.76	6.74/3.83/0.91	0	88.24

5.2. Robustness to tessellations

To test the sensitivity of our method to different tessellations, Bimba model with different tessellations is compared in Fig. 4. Fig. 4 (a) shows the original Bimba model whose triangles vary severely and the mesh of Fig. 4(b) is quasi-regular. The corresponding distortions are not much different and our method is robust to different tessellations. In addition, we also show Fandisk model with a tessellation that varies in element size in Fig. 5. In this example, we remesh the triangles of Fandisk model with different sizes in the left column, and our BLD result in right column. This result shows that our method is insensitive to the anisotropy of meshes.

5.3. Parameter dynamic adjustment

In our experiments, if s is set to be 5 suggested in Fu et al. [15], we observed that it may yield high distortion when there are extremely high or low distortion in the initial guess. This is because the high distortion causes numerical instability in computing the AMIPS energy and its gradient, and the algorithm is easily trapped by a local minimum. To tackle this problem, we use a dynamic adjusting s . We show a comparison on s with AMIPS

[15] and use $s = 5, s = 0.1$ which are suggested in authors' implementation, see Fig. 6. The figure shows that our parameter adjustment scheme is more stable than AMIPS [15] with a fixed s , furthermore, optimization (6) is also necessary to be combined with the parameter adjustment scheme to get a lower worst-case distortion with the same iterations.

5.4. Convergence

Since our energy function is locally convex with respect to each vertex on its one ring neighborhood [13,40], it is effective to apply inexact BCD method to decrease the energy monotonically. Furthermore, our search conditions can keep the energy decreasing sufficiently on the sphere of r_k and prevent overlaps. Therefore, globally, the total energy defined on the whole mesh will decrease relatively rapidly to a minimum value. Fig. 7 shows the log-scale of our energy on per triangle in the first 100 iterations of Hand model and Cow model. It is clear that the energy drops severely during the optimization and it asymptotically goes towards optimal value (i.e. the minimum of our energy on per triangle is 2) with increasing number of iterations. It shows that our algorithm finally converges although the models are with complex geometry.

5.5. Isometric spherical parametrization

We start from a bijective spherical parametrization where both area and angle distortion may be very large, optimize (6) for the first 100 iterations to decrease the average distortion over the whole surface significantly, and then solve (7) with s increasing

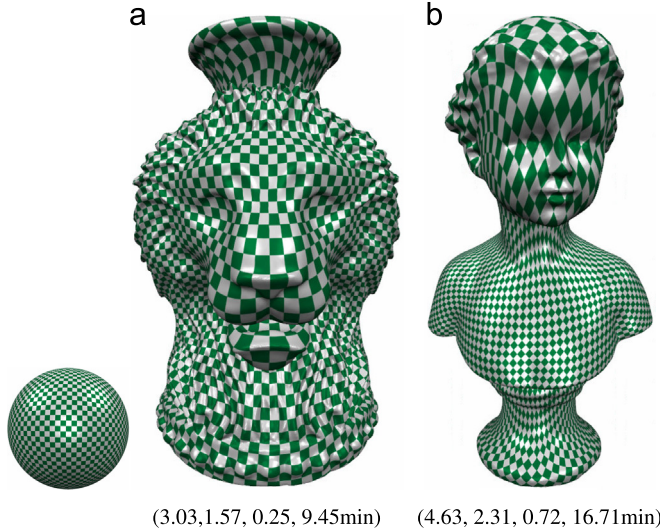


Fig. 10. Isometric spherical parametrizations of two large models with more than 400 K vertices initialized with [50]. The numbers below the figure are D_{\max}^{iso} , $D_{\text{avg}}^{\text{iso}}$, $D_{\text{dev}}^{\text{iso}}$ and running time (in minutes) respectively. (a) Vase-Lion model is about with 400 K vertices and 800 K triangles; (b) Buste model is about with 0.6 M vertices and 1.2 M triangles.

during iterations. For most examples in this paper, we choose the harmonic spherical parametrization as an initial guess and we found our algorithm is not sensitive to initializations discussed in Section 4.2.1. A fair comparison shall be made by scaling the Harmonic result to the radius of BLD. The color encodes the isometric distortion D^{iso} whose minimum is 1 and yellow faces highlight inverted. We also record D_{\max}^{iso} , $D_{\text{avg}}^{\text{iso}}$, the number of triangles whose isometric distortion is greater than the maximal isometric distortion of BLD and number of inverted triangles respectively, see Figs. 8 and 9. The statistics of distortion metrics and timings of models in Figs. 8 and 9 are shown in Table 1. Since we use the author's implementation of Hierarchical [5], we only compare timings with the other two methods. Experiments show that our method outperforms the other methods in terms of both worst case distortion and average distortion on a series of models with simple and complex geometry.

5.5.1. Results on models with simple geometry

Since these models have less curvature change with simple geometry, isometric distortion can be easily minimized and our algorithm converges to a bijective and low distortion parametrization with an optimal sphere radius within 500 iterations. Fig. 8 compares our results with Harmonic [24], Hierarchical [5] and APAP [6] on simple models with the number of vertices under 20 K, and the color bar shows the isometric distortion distribution from 1 to 3. While ARAP [6] produces satisfied average distortion but there is no control on the worst case distortion even overlaps, Hierarchical [5] produces lower area distortion but sacrifices the worst-case/average distortion, our method achieves both the lowest maximal isometric distortion and average isometric distortion among all the methods with comparable computation time.

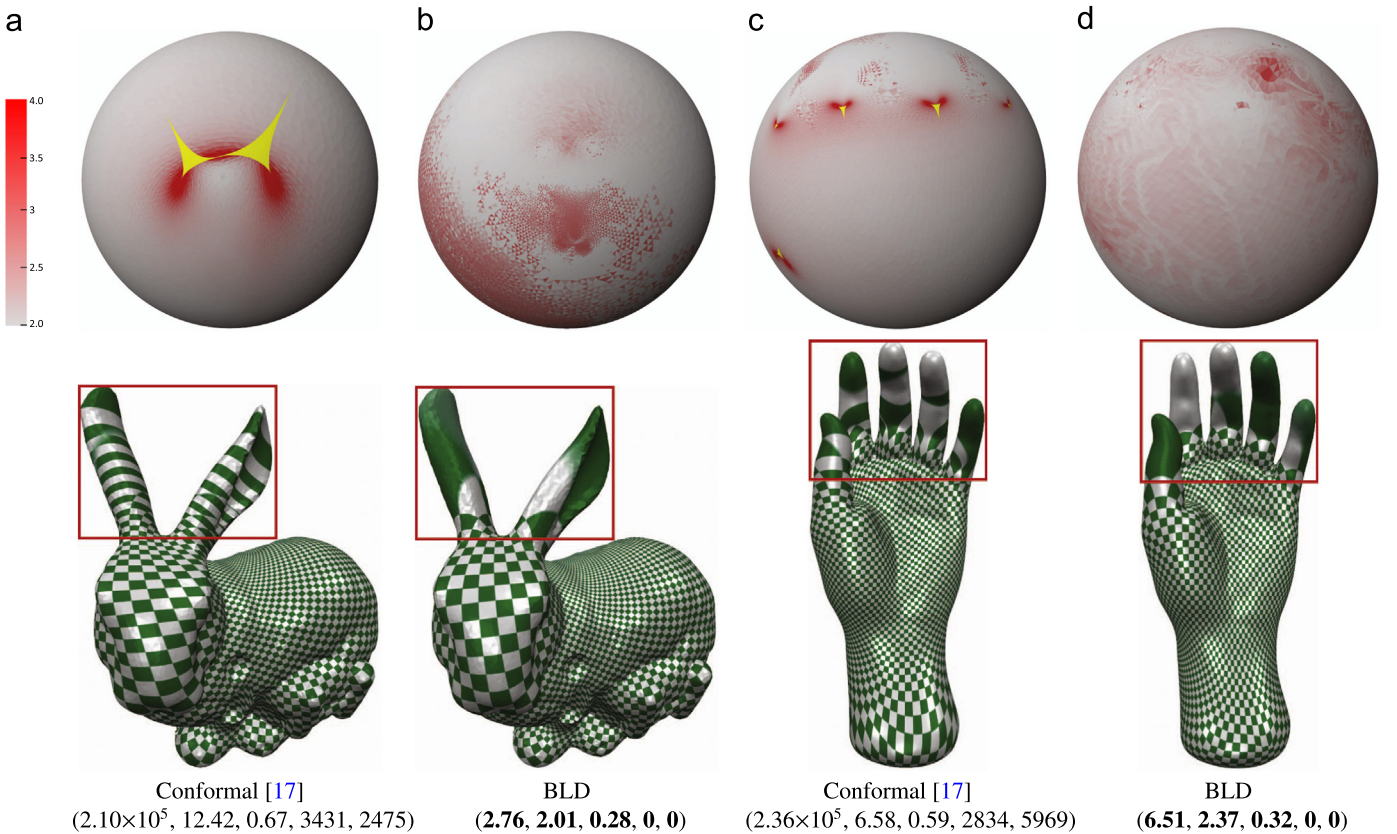


Fig. 11. Comparison of conformal parametrization on Bunny model and the Hand model. The two columns of (a)–(d) show each result with color coding patterns and texture mapping. The color encodes the conformal distortion D^{angle} defined in Eq. (13) and yellow faces highlight inverted. The numbers in brackets below the figure are D_{\max}^{angle} , $D_{\text{avg}}^{\text{angle}}$, $D_{\text{dev}}^{\text{angle}}$, the number of triangles whose conformal distortion is greater than the maximal conformal distortion of BLD and number of inverted triangles. We achieve the Conformal [17] method by the RiemannMapper tool downloaded from the author's personal website.

5.5.2. Results on models with complex geometry

It is challenging to parametrize complex models onto sphere with low isometric distortion as these large models have complex geometry (i.e. with long branches). Fig. 9 compares our results with Harmonic [24], Hierarchical [5] and APAP [6] on complex models with the number of vertices over 20 K, and the color bar shows the isometric distortion distribution from 1 to 8. In addition, statistics of these models is revealed in Table 1. The results show that Harmonic [24] can deal with large models but produce large distortions, especially in feature regions, ARAP [6] cannot produce a bijective parametrization and Hierarchical [5] cannot produce isometric distortion distribution evenly and the maximal isometric is uncontrollable, our method can produce a bijective one with both lowest maximal isometric distortion and lowest average isometric distortion compared with these methods. We also computed isometric parametrizations for several large (more than 400k vertices) meshes with BLD in Fig. 10, and adopt the parallel algorithm [50] to generate an initial guess since Harmonic [24] fails to achieve a valid initialization.

5.6. Conformal spherical parametrization

Similar to the isometric spherical parametrization, we reset $\alpha = 1.0$ and $r = 1.0$ to get the conformal spherical parametrization which is optimized in the same way. This is just the optimization of MIPS energy on the sphere domain. Because of the highly distorted initial guess, we apply our isometric spherical parametrization in the first 100 iterations, then decrease the angle distortion by minimizing MIPS energy. Fig. 11 shows the comparison between the famous Conformal [17] computed by the ReimannMapper from author's homepage and BLD on the Bunny model and Hand model. We apply color coding patterns to the spherical parametrization and texture to the models. The color encodes the conformal distortion D^{angle} defined in Eq. (13) with minimum 2 and yellow faces highlight inverted. The color bar shows the conformal distortion distribution from 2 to 4. The texture results show that Bunny model in (a) severely flips in the ear region and so does to the fingers region of Hand model in (c), while results of BLD in (b) and (d) show that our method is locally angle-preserving, and bijective, especially in the ear of Bunny model and the fingers of Hand model. From the numbers below the figure, we can see that our method can penalize the maximal conformal significantly without foldovers while the Conformal method has no control on the maximal conformal distortion with foldovers.

6. Conclusion

In this paper, we introduce a simple and effective method for bijective spherical parametrization with an optimal radius based on continuous and discrete conformal/isometric mappings, controlling the maximal isometric/conformal distortion and producing an evenly distortion distribution. We formulate this problem as a non-linear constrained optimization problem, solve it using a constrained, and iterative inexact BCD algorithm. Experiments show that our algorithm achieves the lowest maximal distortion and average distortion among all the methods, and the computation speed is comparable to state-of-the-art algorithms.

Our current spherical parametrization has not combined the two optimization (6) and (7) automatically, we hope to search framework where optimization (6) can switch automatically to optimization (7). We also plan to search for more applications based on our BLD results, such as bijective surface mappings or correspondences with low distortion.

Acknowledgements

Thanks to Xin Lin and Ying Li for providing results of the algorithms of [5] and [24]. This work is supported by the National Natural Science Foundation of China (61222206) and the One Hundred Talent Project of the Chinese Academy of Sciences.

Appendix A

In this appendix we introduce the inexact block coordinate descent method in detail. Consider the optimization problem

$$\min_{\mathbf{x} \in \chi} F(\mathbf{x}_1, \dots, \mathbf{x}_s) \quad (\text{A.1})$$

where variable \mathbf{x} is decomposed into s blocks $\mathbf{x}_1, \dots, \mathbf{x}_s$, the set χ of feasible points is assumed to be a closed and block multi-convex subset of \mathbb{R}^n . Suppose that F is strictly convex with respect to variables $\mathbf{x}_i, i = 1, \dots, s$, an inexact standard block coordinate descent method for solving Eq. (A.1) is described as follows.

1. Set the initialization as $(\mathbf{x}_1^0, \dots, \mathbf{x}_s^0)$.

2. For each $i \in \{1, \dots, s\}$, the convex subproblem:

$$\mathbf{x}_i^k = \operatorname{argmin}_{\mathbf{x}_i} F(\mathbf{x}_1^k, \dots, \mathbf{x}_{i-1}^k, \mathbf{x}_i^{k-1}, \mathbf{x}_{i+1}^{k-1}, \dots, \mathbf{x}_s^{k-1})$$

is solved by a local linear approximation from only one step of gradient descent instead of local Newton iterations.

3. The algorithm terminates when stopping criterion is satisfied, and return $(\mathbf{x}_1^k, \dots, \mathbf{x}_s^k)$. Otherwise, go to Step 2.

Appendix B

In this appendix, we compute the gradient of the energy in Eqs. (4) and (5) with respect to a vertex \mathbf{u}_v , denoted as $\nabla_{\mathbf{u}_v} E_1$ and $\nabla_{\mathbf{u}_v} E_2$ respectively. It is clear that

$$\nabla_{\mathbf{u}_v} E_1(\mathbf{u}) = \frac{1}{2} \sum_{\tau \in N(\mathbf{u}_v)} \nabla_{\mathbf{u}_v} E_1^\tau,$$

$$\nabla_{\mathbf{u}_v} E_2(\mathbf{u}) = \frac{1}{2} \sum_{\tau \in N(\mathbf{u}_v)} \nabla_{\mathbf{u}_v} E_2^\tau,$$

Thus, we only need to compute the gradient on each triangle τ : $\nabla_{\mathbf{u}_v} E_1^\tau$ and $\nabla_{\mathbf{u}_v} E_2^\tau$. Suppose triangle $\tau = \mathbf{u}_{v-} \mathbf{u}_v \mathbf{u}_{v+}$, then

$$\nabla_{\mathbf{u}_v} E_1^\tau = \frac{2}{a_\tau} (\cot \theta_{v+} \ell_{v+} - \cot \theta_{v-} \ell_{v-}) - \frac{E_1^\tau \ell_v^\perp}{a_\tau},$$

$$\nabla_{\mathbf{u}_v} E_2^\tau = \frac{a_\tau^2 - A_\tau^2 \ell_v^\perp}{A_\tau a_\tau^2},$$

where θ_v is the angle at the v -vertex, ℓ_v is the opposite edge of v -vertex and ℓ_v^\perp is the 90° counter-clockwise rotation of ℓ_v , see Fig. B1.

At last, the gradient of the energy in Eq. (7) can be obtained easily by the chain rule.

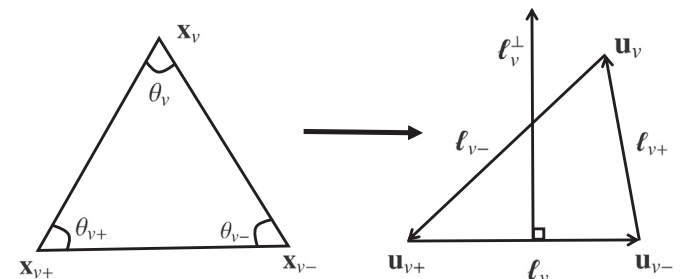


Fig. B1. Computation on each original triangle and parametrization triangle.

References

- [1] Gu X, Wang Y, Chan TF, Thompson PM, Yau ST. Genus zero surface conformal mapping and its application to brain surface mapping. *IEEE Trans Med Imaging* 2004;23(8):949–58.
- [2] Li H, Hartley R. Conformal spherical representation of 3d genus-zero meshes. *Pattern Recognit* 2007;40(10):2742–53.
- [3] Li X, He Y, Gu X, Qin H. Curves-on-surface: a general shape comparison framework. In: Proceedings of the IEEE international conference on shape modeling and applications 2006; 2006. p. 352–7.
- [4] Zayer R, Rossin C, Seidel H.P. Curvilinear spherical parameterization. In: Proceedings of the IEEE international conference on shape modeling and applications 2006; 2006. p. 11–9.
- [5] Wan S, Ye T, Li M, Zhang H, Li X. An efficient spherical mapping algorithm and its application on spherical harmonics. *Sci China Inf Sci* 2013;56(9):1–10.
- [6] Wang C, Liu Z, Liu L. As-rigid-as-possible spherical parametrization. *Graph Models* 2014;76(5):457–67.
- [7] Lipman Y. Bounded distortion mapping spaces for triangular meshes. *ACM Trans Graph* 2012;31(4):108:1–13.
- [8] Aigerman N, Lipman Y. Injective and bounded distortion mappings in 3d. *ACM Trans Graph* 2013;32(4):106–18.
- [9] Kovalsky SZ, Aigerman N, Basri R, Lipman Y. Controlling singular values with semidefinite programming. *ACM Trans Graph* 2014;33(4):68:1–13.
- [10] Kovalsky SZ, Aigerman N, Basri R, Lipman Y. Large-scale bounded distortion mappings. *ACM Trans Graph (SIGGRAPH ASIA)* 2015;34(6):191:1–10.
- [11] Jin Y, Huang J, Tong R. Remeshing-assisted optimization for locally injective mappings. *Comput Graph Forum (SGP)* 2014;33(5):269–79.
- [12] Weber O, Zorin D. Locally injective parametrization with arbitrary fixed boundaries. *ACM Trans Graph* 2014;33(4):75:1–12.
- [13] Hormann K, Greiner G. MIPS: An efficient global parametrization method. In: Curve and surface design: Saint-Malo 1999; 2000. p. 153–62.
- [14] Degener P, Meseth J, Klein R. An adaptable surface parameterization method. In: Proceedings of the 12th international meshing roundtable; 2003. p. 201–13.
- [15] Fu XM, Liu Y, Guo B. Computing locally injective mappings by advanced mips. *ACM Trans Graph* 2015;34(4):71–82.
- [16] Smith J, Schaefer S. Bijective parameterization with free boundaries. *ACM Trans Graph* 2015;34(4):70:1–10:9.
- [17] Gu X, Yau ST. Global conformal surface parameterization. In: Proceedings of the 2003 Eurographics/ACM SIGGRAPH symposium on geometry processing; 2003. p. 127–37.
- [18] Floater M, Hormann K. Surface parameterization: a tutorial and survey. In: Advances in multiresolution for geometric modelling. Mathematics and visualization; 2005. p. 157–86.
- [19] Sheffer A, Praun E, Rose K. Mesh parameterization methods and their applications. *Found Trends Comput Graph Vis* 2006;2(2):105–71.
- [20] Tutte WT. How to draw a graph. *Proc Lond Math Soc* 1963;13(3):743–68.
- [21] Floater MS. One-to-one piecewise linear mappings over triangulations. *Math Comput* 2003;72(242):685–96.
- [22] Gotsman C, Gu X, Sheffer A. Fundamentals of spherical parameterization for 3d meshes. *ACM Trans Graph (Proc SIGGRAPH)* 2003;22(3):358–63.
- [23] Saba S, Yavneh I, Gotsman C, Sheffer A. Practical spherical embedding of manifold triangle meshes. In: Proceedings of the IEEE international conference on shape modeling and applications 2005; 2005. p. 256–65.
- [24] Li Y, Yang Z, Deng J. Spherical parametrization of genus-zero meshes by minimizing discrete harmonic energy. *J Zhejiang Univ Sci A* 2006;7(9):1589–95.
- [25] Jin M, Wang Y, Yau ST, Gu X. Optimal global conformal surface parameterization. In: Proceedings of the conference on visualization '04; 2004. p. 267–74.
- [26] Sheffer A, Gotsman C, Dyn N. Robust spherical parameterization of triangular meshes. *Computing* 2004;72(1–2):185–93.
- [27] Friedel I, Schröder P, Desbrun M. Unconstrained spherical parameterization. *J Graph GPU Game Tools* 2007;12(1):17–26.
- [28] Schüller C, Kavan L, Panozzo D, Sorkine-Hornung O. Locally injective mappings. *Comput Graph Forum (SGP)* 2013;32(5):125–35.
- [29] Sorkine O, Cohen-Or D, Goldenthal R, Lischinski D. Bounded-distortion piecewise mesh parameterization. In: Proceedings of the conference on visualization'02; 2002. p. 355–62.
- [30] Alexa M, Cohen-Or D, Levin D. As-rigid-as-possible shape interpolation. In: Proceedings of the 27th annual conference on computer graphics and interactive techniques; 2000. p. 157–64.
- [31] Igarashi T, Moscovich T, Hughes JF. As-rigid-as-possible shape manipulation. *ACM Trans Graph* 2005;24(3):1134–41.
- [32] Solomon J, Ben-Chen M, Butscher A, Guibas L. As-killing-as-possible vector fields for planar deformation. *Comput Graph Forum* 2011;30(5):1543–52.
- [33] Sorkine O, Alexa M. As-rigid-as-possible surface modeling. In: Proceedings of the fifth Eurographics symposium on geometry processing; 2007. p. 109–116.
- [34] Liu L, Zhang L, Xu Y, Gotsman C, Gortler SJ. A local/global approach to mesh parameterization. In: Proceedings of the symposium on geometry processing. SGP '08; 2008. p. 1495–504.
- [35] Freitag LA, Knupp PM. Tetrahedral mesh improvement via optimization of the element condition number. *Int J Numer Methods Eng* 2002;53(6):1377–91.
- [36] Paillet GP, Poulin P. As-conformal-as-possible discrete volumetric mapping. *Comput Graph* 2012;36(5):427–33.
- [37] Do Carmo MP, Do Carmo MP. Differential geometry of curves and surfaces. Pearson, Englewood Cliffs: Prentice-hall, 1st edition; 1976.
- [38] Eisenhart LP. Riemannian geometry. 1st edition. Princeton: Princeton University Press; 1997.
- [39] Kreyszig E. Differential geometry. Dover, New York, 1st editions; 1991.
- [40] Jiao X, Wang D, Zha H. Simple and effective variational optimization of surface and volume triangulations. *Eng Comput* 2011;27(1):81–94.
- [41] Knupp PM. Achieving finite element mesh quality via optimization of the jacobian matrix norm and associated quantities. Part I—a framework for surface mesh optimization. *Int J Numer Methods Eng* 2000;48(3):401–20.
- [42] Munson T. Mesh shape-quality optimization using the inverse mean-ratio metric. *Math Program* 2007;110(3):561–90.
- [43] Freitag Diachin L, Knupp P, Munson T, Shontz S. A comparison of two optimization methods for mesh quality improvement. *Eng Comput* 2006;22(2):61–74.
- [44] Ivanenko SA. Harmonic mappings. In: Handbook of grid generation; 1999.
- [45] Garimella RV, Shashkov MJ, Knupp PM. Triangular and quadrilateral surface mesh quality optimization using local parametrization. *Comput Methods Appl Mech Eng* 2004;193(9):913–28.
- [46] Pinkall U, Polthier K. Computing discrete minimal surfaces and their conjugates. *Exp Math* 1993;2(1):15–36.
- [47] Sorkine O, Cohen-Or D, Goldenthal R, Lischinski D. Bounded-distortion piecewise mesh parameterization. In: Proceedings of the conference on visualization'02; 2002. p. 355–62.
- [48] Xu Y, Yin W. A block coordinate descent method for regularized multiconvex optimization with applications to nonnegative tensor factorization and completion. *SIAM J Imaging Sci* 2013;6(3):1758–89.
- [49] Lipman Y. Bijective mappings of meshes with boundary and the degree in mesh processing. *SIAM J Imaging Sci* 2014;7(2):1263–83.
- [50] Athanasiadis T, Fudos I. Parallel computation of spherical parameterizations for mesh analysis. *Comput Graph* 2011;35(3):569–79.